Lagrangian Flow Structures in 3D AC Electro-Osmotic Microflows

M. F. M. Speetjens *, H. N. L. de Wispelaere, A.A. van Steenhoven

* Corresponding author: m.f.m.speetjens @tue.nl
Energy Technology Laboratory, Eindhoven University of Technology, The Netherlands

Abstract Flow forcing by AC electro-osmosis (ACEO) is a promising technique for actuation and manipulation of microflows. Utilisation to date mainly concerns pumping and mixing. However, emerging micro-fluidics applications demand further functionalities. The present study explores first ways by which to systematically realise this in three-dimensional (3D) microflows using ACEO. This exploits the fact that continuity "organises" Lagrangian fluid trajectories into coherent structures that geometrically determine the transport properties. 3D Lagrangian flow structures typically comprise families of concentric (closed) streamtubes, acting both as transport barriers and transport conduits, embedded in chaotic regions. Representative case studies demonstrate that ACEO, possibly in combination with other forcing mechanisms, has the potential to tailor these features into multi-functional Lagrangian flow structures for various transport purposes. This may pave the way to "labs-within-a-channel" that offer the wide functionality of labs-on-a-chip yet within one microflow instead of within an integrated system.

Keywords: 3D ACEO Microflows, Lagrangian Transport Analysis, 3D Flow Topology

1. Introduction

Flow forcing by AC electro-osmosis (ACEO) is a promising technique for actuation and manipulation of micro-flows (Squires 2009, Stone et al., 2004). Primary micro-fluidic applications to date include pumping (Bazant & Ben, 2006, Kuo & Liu, 2008, Ramos et al., 2005) and mixing (Chen et al., 2009, Nguyen & Wu, 2005). However, emerging (lab-on-a-chip) technologies for e.g. molecular analysis and biotechnology demand further functionalities including establishment of specific temperature or concentration fields and targeted delivery of heat and mass in designated flow regions (Weigl et al., 2008, Mills et al., 2008). ACEO seems particularly suited for realisation of such multi-functional microflows in that clever design of electrode layout and geometry in combination with variable spatio-temporal AC signals offers great control over the internal flow (Ramos et al., 2005, Squires, 2009). This motivates the present study, which explores first ways by which to systematically achieve generic transport functionalities in three-dimensional (3D) microflows using ACEO.

Fundamental to micro-fluidic transport is that it happens under laminar flow conditions (Ottino & Wiggins, 2004). This implies a strong disparity between a flow and its transport properties in that simple and regular flow patterns may coexist with complicated transport properties. (Well-known example is chaotic fluid advection in simple flows; Aref, 2002.) This advances a Lagrangian representtation as the most natural description for laminar transport (Ottino & Wiggins, 2004). Continuity "organises" the Lagrangian fluid trajectories into specific coherent structures that geometrically determine the transport properties Cartwright et al, 1996, Speetjens et al., 2004). This notion admits visualisation and analysis of laminar transport by identification of such "elementary building blocks." Moreover, this fundamental geometric organisation - in principle - enables systematic creation and destruction of coherent structures for specific transport purposes.

Studies on micro-fluidic Lagrangian transport primarily concern the transverse mixing of axial fluid streams in 3D steady flow within infinite micro-channels (Chen et al., 2009, Nguyen & Wu, 2005). The present study demonstrates that ACEO has the potential for manipulation of transport properties beyond

that of destruction of (tubular) transport barriers for mixing purposes - even in a standard periodic micro-channel. This exploits the fact that incompressible 3D steady flows devoid of a global uni-directional component in essence consist of multiple flow regions that each separately exhibit the Hamiltonian dynamics described above for inline (micro-)mixers. The generic Lagrangian flow structure, in consequence, encompasses multiple families of tubular transport barriers embedded within chaotic regions. The particular arrangement and states of disintegration of said tubes depends essentially on the flow forcing, however. This affords promising practical opportunities in that ACEO, possibly in combination with another forcing (e.g. pressure gradients or DC electro-osmosis), thus facilitates systematic manipulation of the Lagrangian flow structure for a wide range of transport purposes. This paves the way to a much greater functionality than pumping and mixing alone. Moreover, it offers great flexibility by (in principle) enabling the realisation of multiple Lagrangian flow structures within one micro-channel.

This paper is organised as follows. Sec. 2 introduces the configuration investigated here. The theoretical framework for Lagrangian flow structures is outlined in Sec. 3. The basic Lagrangian composition of ACEO flows is examined in Sec. 4 and its emergence in more complex micro-fluidic systems is demonstrated in Sec. 5. Conclusions are in Sec. 6.

2. Problem definition

The flow domain consists of a 3D rectangular channel *V: [x,y,z]=[0, 2L]x[0,H]x[0,L]* with periodic inlet (*x=0*) and outlet (*x=2L*). Two electrodes of width W_e and spacing $W_s=L-W_e$ are placed parallel to the z-axis at the bottom wall within intervals $W_s/2<x<L-W_s/2$ and $L+W_s/2<x<2L-W_s/2$ (Fig. 1a). ACEO triggered by these electrodes induces a slip velocity on the bottom wall (Fig. 1b) that sets up an internal flow comprising electrode-wise pairs of counter-rotating vortices (Fig. 1a) and small vortices near the electrode edges (not shown).

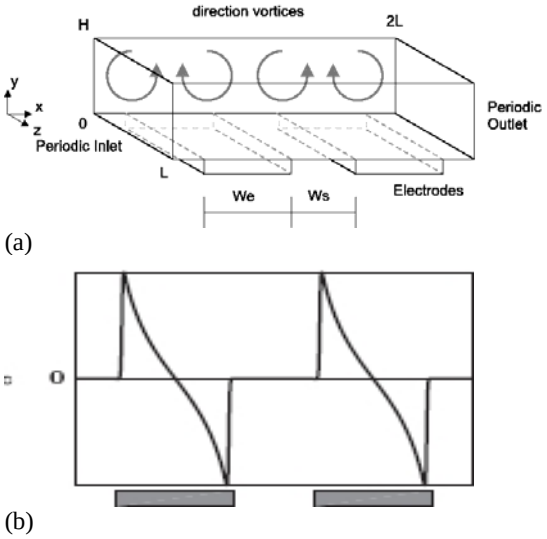

Fig. 1. 3D ACEO configuration: (a) periodic flow domain including electrodes; (b) typical axial slip velocity on bottom wall.

ACEO is described by the linear model according to Ramos et al (2005). This hinges on two assumptions: (i) the voltage $V(t)=V_0\sin(\omega t)$, with V_0 the amplitude and ω the AC frequency, applied to the electrodes is small enough to prevent electrolysis; (ii) the electric double layer (EDL) is in a quasi-equilibrium (i.e. $\omega << \tau_{EDL}^{-1}$, with $\tau_{EDL}=\varepsilon/\sigma$ the relaxation time of the cyclic EDL charging, ε the permittivity and σ the conductivity). This implies that the EDL acts as an ideal capacitor (capacitance C_{DL}) and means that the electrical potential Φ in the bulk fluid is described by the potential problem

$$\nabla^2\Phi = 0\,, \quad \frac{\sigma}{C_{DL}}\frac{\partial\Phi}{\partial y}\bigg|_e = \frac{\partial}{\partial t}(\Phi - V)\big|_e\,, \quad (1)$$

completed by condition $\partial\Phi/\partial y\big|_g = 0$ and $\Phi\big|_{y=H} = 0$, where "e" and "g" denote electrode and glass segments on the bottom wall, respectively, and $\Phi\big|_{x=0} = \Phi\big|_{x=2L}$ due to the periodic inlet-outlet. Moreover, the arrangement of the electrodes parallel to the *z*-axis means transverse variations are absent, reducing the electro-kinetic system to a two-dimensional (2D) problem for $\Phi = \Phi(x, y)$.

The ion flux induced by the electric field

gives rise to a slip velocity directly above the electrodes that effectively acts as a "driving wall" for the fluid. However, the AC frequency ω is such that the fluid cannot follow the instantaneous changes in ion propagation direction and, in consequence "feels" only the time-averaged slip velocity

$$\left\langle u_{slip} \right\rangle = -\frac{\varepsilon\Lambda}{4\mu}\frac{\partial}{\partial x}(|\Phi - V_0|^2), \qquad (2)$$

with $\Lambda = C_{DL}/C_D$ the ratio of capacitances of EDL and diffusive layer. The negligible potential drop at the glass/electrolyte interfaces results in a zero slip velocity (Ramos et al., 2005).

The three-dimensional (3D) flow field $\vec{u} = \vec{u}(x, y, z)$ is governed by the steady incompressible Navier-Stokes equations

$$\nabla \cdot \vec{u} = 0, \quad \vec{u} \cdot \nabla \vec{u} = -\frac{1}{\rho}\nabla p + \nu \nabla^2 \vec{u}, \qquad (3)$$

with p the dynamic pressure, ρ the fluid density and ν its kinematic viscosity. Here spatial periodicity, similar as before, means $\vec{u}_{x=0} = \vec{u}\big|_{x=2L}$. The flow is subject to the no-slip condition $\vec{u} = \vec{0}$ on top wall ($y=H$), sidewalls ($z=0,1$) and between the electrodes at the bottom wall. The time-averaged slip velocity (2) is imposed on the electrodes: $\vec{u}\big|_e = (\langle u_{slip} \rangle, 0, 0)$. The electro-kinetic phenomena manifests themselves only through this slip velocity; internal electric body forces are absent in the present approximation. Hence only a one-way coupling between electro-kinetics and fluid dynamics exists.

The corresponding non-dimensional form follows from rescaling the relevant quantities via $x'=x/L$, $t'=t/\tau_{RC}$, $\Phi'=\Phi/V_0$, $V'=V/V_0$, $\vec{u}' = \vec{u}/U$ and $p'=pL/\rho\nu U$, with L as before, $\tau_{RC}=C_{DL}L/\sigma$ and $U=max(<u_{slip}>)$. (The pressure scale stems from assuming that a balance between pressure and viscous forces dominates the momentum equation.) This readily yields the associated non-dimensional domain $V':[x,y,z]=[0,2]x[0,D]x[0,1]$, with $D=H/L$ the vertical aspect ratio $W_e'=W_e/L$ and $W_s'=W_s/L$ as corresponding electrode dimensions. Substitution into (1) and (2) thus exposes the Reynolds number $Re=UL/\nu$ and the dimensionless AC frequency $\omega'=\omega\tau_{RC}$ as relevant non-dimensional parameters. These are partially fixed at $D=0.5$, $W_e'=0.6$, $W_s'=0.4$ and $\omega'=1$, leaving Re as single system parameter in the analysis below. Further degrees of freedom include the electrode configuration and combination with other forcing mechanisms. Refer to Speetjens et al. (2011) for details on the non-dimensionalisation.

Numerical simulations are performed by a combination of dedicated and commercially-available CFD tools. The electro-kinetic problem is resolved by a dedicated spectral solver based upon Fourier-Chebyshev polynomials (Canuto et al., 1988). The flow field is simulated by way of the commercial CFD package FLUENT. The kinematic equation is integrated via a dedicated tracking code employing a third-order Taylor-Galerkin scheme. Both dedicated algorithms are implemented in MATLAB. Consult Speetjens et al. (2011) for an elaborate description of the numerical treatment including a performance analysis.

3. Lagrangian transport analysis by Hamiltonian mechanics

Laminar transport is an essentially Lagrangian phenomenon (qualitatively) determined by the topological properties of the fluid trajectories. The continuity constraint $\nabla \cdot \vec{u} = 0$ "organizes" these trajectories into coherent structures that collectively define the flow topology and geometrically determine fluid advection (Speetjens et al, 2004).

The motion of fluid parcels is governed by the 3D autonomous kinematic equation

$$\frac{d\vec{x}}{dt} = \vec{u} \quad \Rightarrow \quad \vec{x}(t) = \vec{\Phi}(\vec{x}_0), \qquad (4)$$

describing the Lagrangian fluid trajectories originating from initial positions $\vec{x}_0$. These trajectories coincide with streamlines of $\vec{u}$ in the present study due to steady flow. Continuity enables (local) recasting of (4) into the 2D Hamiltonian system

$$\frac{d\eta}{d\xi} = \frac{\partial H}{\partial \varsigma}, \; \frac{d\varsigma}{d\xi} = -\frac{\partial H}{\partial \eta} \Rightarrow \vec{x}'(\xi) = \vec{\Phi}'(\vec{x}_0'), \quad (5)$$

with $\vec{x}'=(\eta,\varsigma)$, everywhere outside stagnation points $\vec{u}=\vec{0}$ via (local) coordinate transformation $F:(x,y,z)\rightarrow(\eta,\varsigma,\xi)$ (Bajer, 1994, Speetjens et al., 2006a). Function $H(\eta,\zeta,\xi)$ represents the Hamiltonian; variables $x'=(\eta,\zeta)$ and ξ define the corresponding spatial and temporal coordinates, respectively. Thus the present ACEO flows, save in the proximity of (possible) stagnation points, in essence exhibit Hamiltonian dynamics. This has fundamental ramifications for composition and behaviour of the flow topology.

The key coherent structures of Hamiltonian flow topologies are tori. In system (5) they appear as families of concentric closed orbits defining island-like structures ("elliptic islands") in the 2D (η,ζ)-domain and tubes in the 3D space-time domain (η,ζ,ξ) (Wiggins & Ottino, 2004). In the 3D spatially-periodic steady flow they may emerge in two kinds. First, as stream tubes connecting the periodic inlet-outlet. Cross-sections (y,z) and axial coordinate x then correspond (yet *not* identify) with (η,ζ) and ξ, respectively, meaning the axial flow u_x acts as a fictitious evolution in time. Second, as closed stream tubes within V (Speetjens et al., 2006a,b). Here cross-section and secondary axis of the tori correspond with (η,ζ) and ξ, respectively. Furthermore, the closedness of the tori implies a time-periodic associated 2D Hamiltonian system, i.e. $H(\eta,\zeta,\xi)=H(\eta,\zeta,\xi+\tau)$, with τ some (typically family-dependent) period time. Streamlines are limit cases in that they correspond to tori with cross-sections collapsing on a single point. Both kinds of physical appearances of tori are illustrated in Fig. 2; heavy curves outline the 2D (η,ζ)-domain.

The periodic evolution within families of tori admits reduction of the continuous flow in the Hamiltonian formulation (5) to a map

$$\vec{x}'_{k+1}=\vec{\Phi}'_{\tau}(\vec{x}'_k),\quad \vec{x}'_k=\vec{x}'(k\tau), \qquad (6)$$

with the sequence of positions $X(\vec{x}'_0)=[\vec{x}'_0,\vec{x}'_1,\vec{x}'_2,...]$ within the 2D (η,ζ)-domain (heavy curves in Fig.2). This constitutes the so-called Poincaré section of the trajectory originating from position $\vec{x}'_0$ (Wiggins & Ottino, 2004). Time levels $\xi=k\tau$ $(k=0,1,...)$ correspond with fixed spatial cross-sections of the 3D stream tubes.

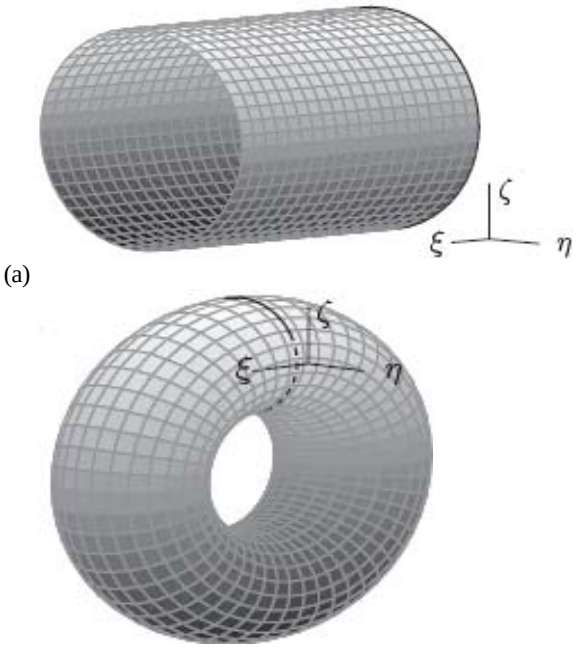

(a)

(b)

Fig. 2. Two kinds of physical appearance of tori in 3D steady flows: (a) stream tubes connecting periodic inlet-outlet; (b) closed stream tubes in the domain interior.

The 3D transport properties are inextricably linked to Hamiltonian response scenarios of the flow topology to perturbation introduced by e.g. the flow forcing. For "weak" perturbations three basic responses may occur tori (Cartwright et al., 1996):

(i) Perturbation of closed streamlines causes coalescence into families of tori.

(ii) Perturbation of rational tori causes break-up into multiple families of tori embedded in chaotic bands according to the Poincaré-Birkhof theorem.

(iii) Perturbation of irrational tori causes survival in a slightly deformed manner according to the KAM theorem.

Tracers on a rational torus resume initial positions after a finite number of revolutions and thus describe closed streamlines wound around its surface. Tracers on an irrational torus describe non-closed streamlines that densely fill its surface. The response to

"strong" perturbations is essentially nonlinear and case-specific and *may* yet not *must* result in progressive disintegration of surviving tori into a state of total chaos. Thus flow topologies basically consist of (remnants of) tori situated in a chaotic environment and subject to the above response scenarios. This enables a systematic strategy for Lagrangian transport studies.

4. Flow topology in basic ACEO flows

The study by Speetjens et al (2011) revealed that the basic ACEO flow per electrode accommodates two counter-rotating vortices consisting of closed streamlines in case of symmetric slip velocity and non-inertial flow (*Re=0*). Asymmetric slip velocity per vortical structure, as happening in realistic situations (Fig. 1b), and/or fluid inertia break this symmetry and thus trigger the Hamiltonian response scena-rios described in Sec. 3 that underly formation and (partial) disintegration of toroidal struc-tures. This is demonstrated in Fig. 3 by way of the flow topology for *Re=100*. Each electrode sets up pairs of counter-rotating vortices. This, on account of symmetries, gives rise to sym-metric arrangements of quadruples of coherent structures in the interval $0<x<1$, shown in Fig. 3a, and an identical arrangement in the interval $1<x<2$ (not shown). The topology comprises the elementary building blocks of Hamiltonian topologies: ring tori (bright); tori with winding number higher than one emanating from disintegrated ring tori (dark); chaotic sea (black).[1] Fig. 3b gives the intersection of these topological features with the planes $x=0.25$ and $x=0.75$ on either side of the symmetry plane $z=0.5$ (dashed outline in Fig. 3a). This symmetry plane acts as a transport barrier to tracer migration and effectively divides the micro-channel into two disconnected parallel ducts $0<z<0.5$ and $0.5<z<1$. Tracers within each duct are either entrapped within tori or randomly wander around within the chaotic region formed by merger of chaotic seas of (disintegrated) neighbouring tori. This chaotic region facilitates free passage of tracers throughout the entire duct. Such tracers typically remain temporarily entangled in a vortical region before changing over to the adjacent region by; this intermittent behaviour of temporary entrapment and vortex switching repeats itself *ad infinitum* and brings about a random motion resembling that of a pinball machine.

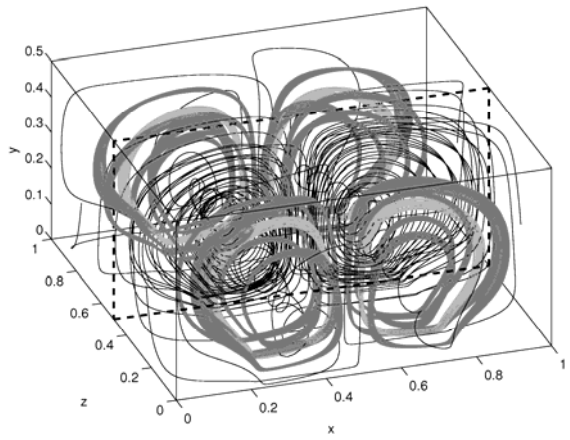

(a)

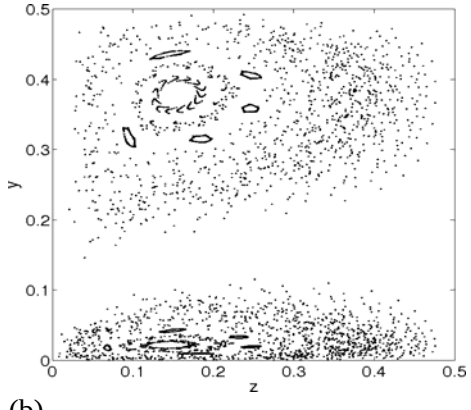

(b)

Fig. 3. Typical topological make-up of the basic ACEO flow demonstrated for *Re=100*: (a) perspective view on ring tori (bright), tori emanating from disintegrated ring tori (dark) and chaotic sea (black). The dashed frame outlines the symmetry plane $z=0.5$; (b) intersections with planes $x=0.25$ and $x=0.75$ on either side of this plane.

[1] The winding number *W* represents the number of revolutions required for completing a full loop on a closed orbit. For the standard (or "ring") torus $W=1$; for tori formed by Hamiltonian breakdown generally $W>1$.

5. Flow topologies in flows due to combined ACEO and axial forcings

Functionality of micro-fluidic systems admits further expansion by combining ACEO forcing with other forcings. This is demonstrated below for ACEO forcing by electrode pairs on the bottom walls in conjunction with axial forcing by a pressure gradient in the non-inertial limit *Re=0*. (This is equally representative for axial forcing due to electro-osmosis.) The non-inertial momentum balance admits linear decomposition of the total flow into ACEO component $\vec{u}$ and pressure-driven component $\vec{u}_p$ following

$$\vec{u}_{tot} = \vec{u} + \beta\vec{u}_p, \qquad (7)$$

with $\vec{u}$ as before and $\vec{u}_p = (u_x,0,0)$ given by the Poiseuille flow

$$u_x(y,z) = \frac{786}{\pi^4}\sum[mn(4m^2+n^2)]^{-1}\sin(2\pi my)\sin(\pi nz), \qquad (8)$$

with $1 \le m,n \le \infty$ and *m,n* odd, for ducts with rectangular cross-sections (Hunt, 1965).[2] The latter yields unit mean flow, meaning that parameter β represents the ratio of characteristic axial to ACEO-driven flows. Hence, growing β signifies diminishing ACEO-driven component *v.v.* Limit $\beta=0$ corresponds with pure ACEO flow and gives rise to electrode-wise quadruples of vortices similar to those shown in Fig. 3; limit $\beta \to \infty$ corresponds with purely axial flow. Augmenting axial forcing by increasing β causes transition from former to latter limit.

Non-zero axial flow ($\beta>0$) introduces axial-wise symmetry breaking and thus brings about a fundamental change in topological make up. This is demonstrated in Fig. 4 for $\beta=0.1$. The original tori partially survive in a deformed manner (black and blue). The outer tori associated with the vortical structure in interval $0<x<0.5$ (blue) "open up" at their top side in that their constituent streamlines are on the downstream side deflected towards the neigbouring electrode, envelop the surviving tori in interval $0.5<x<1$ (black) and subsequently reconnect with the remnants of said tori via the periodic inlet-outlet (cyan). This partial disintegration of tori in fact underlies formation of a common chaotic region reminiscent of that surrounding the tori in Fig. 3. Moreover, this results in the emergence of families of stream tubes connecting periodic inlet-outlet and constituting concentric serpentine-like channels alternately running above and beneath surviving tori (red and magenta). These stream tubes are topologically equivalent to (disintegrated) tori in that tracers periodically return to the same cross-section and, in consequence, exhibit the same dynamics as before. Hence, they constitute the tori of the first kind according to Sec. 3 and are in fact hallmarks of the flow topology in axially-driven duct flows (Speetjens et al, 2006a). Coexistence of tori of first and second kinds thus reflects the dual nature of the present flow in that it contains elements of both vortical and uni-directional flows. Thus the present flow exhibits a richer topology than the purely ACEO-driven flows considered above.

Increasing the axial flow inflates the newly-formed longitudinal tori and promotes further disintegration of the original tori. Thus the flow topology gradually transforms into an intricate arrangement of multiple families of tori with various orientations and embedded in a common chaotic sea. However, it remains composed of the same elementary building blocks as before, which is a direct consequence of the (region-wise) Hamiltonian structure of the equations of motion (Sec. 3). Intermediate (chaotic) regions nonetheless seem to accommodate truly 3D dynamics; local defects in tori appear to exist in the area pointed out by the arrow in Fig. 4(d) that facilitate random switching similar to the behaviour observed in other 3D steady flows (Bajer & Moffat, 1990, Neishtadt & Vasiliev, 1999).

[2] Solution (8) readily follows from the analytical solution for magnetohydrodynamic derived in Hunt (1965) upon disabling magnetic forcing.

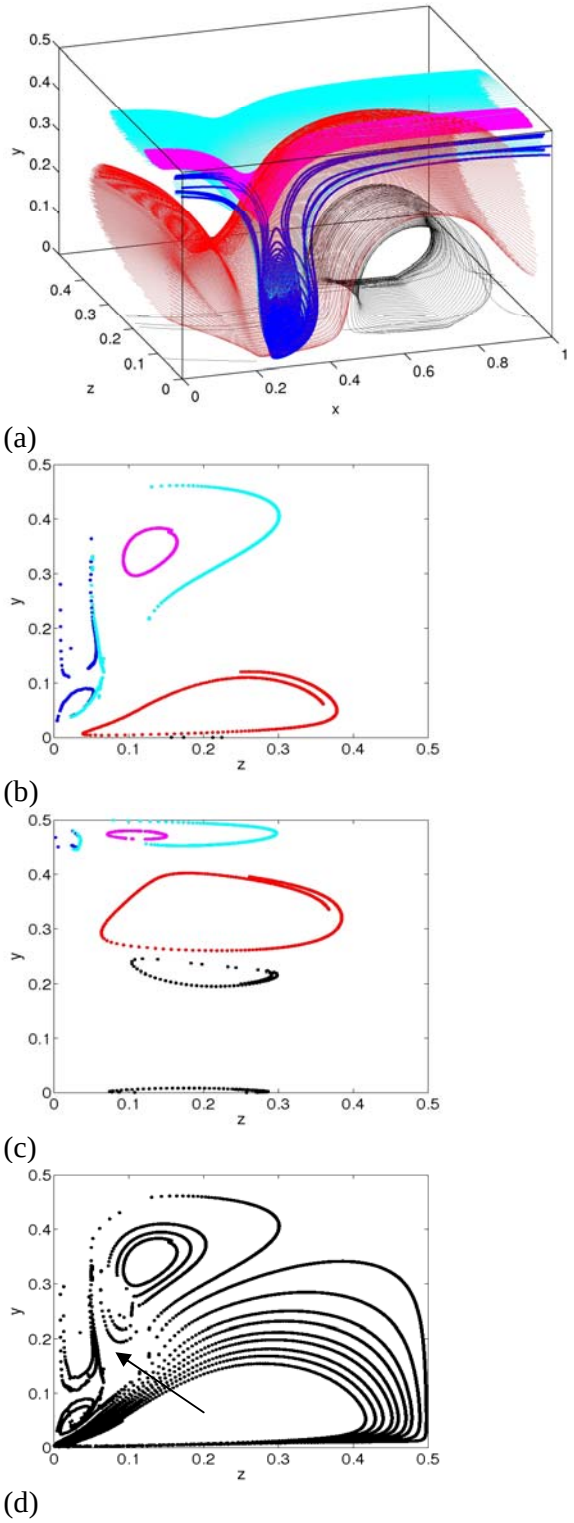

Fig. 4. Flow topology due to combined ACEO and axial forcing (β=0.1): (a) 3D streamlines delineating multiple families of tori (red/magenta) and disintegrating tori (black/blue/cyan); (b) intersection at x=0.25; (c) intersection at x=0.75; (d) intersection at x=0.25 including additional 3D streamlines.

6. Conclusions

The present study concerns numerical simulation and analysis of the Lagrangian flow structure in ACEO micro-flows. This structure geometrically determines the transport properties in essentially laminar flows as e.g. micro-fluidics and thus insight into its composition is of fundamental importance to systematic utilisation of ACEO forcing for micro-mixers, micro-reactors and lab-on-a-chip applications. The analysis considers a basic periodic micro-channel accommodating a 3D steady flow set up by ACEO forcing and in some cases including an axial background flow. Numerical simulations are performed by a combination of dedicated and commercially-available CFD tools.

Incompressibility admits (local) transformation of the 3D Lagrangian equations of motion into 2D non-autonomous Hamiltonian systems everywhere outside stagnation points. Thus the present ACEO flows, save in the proximity of said points, in essence exhibit Hamiltonian dynamics, which has fundamental ramifications for the flow topology. The key coherent structures of Hamiltonian flow topologies are tori, which in the present class of 3D steady flows may emerge in two kinds: (i) stream tubes connecting the periodic inlet-outlet; (ii) closed stream tubes within the domain interior. These tori typically are in a (partial) state of disintegration due to perturbations induced by the flow forcing. This disintegration follows very specific Hamiltonian scenarios and results in the characteristic Hamiltonian topology comprising (remnants of disintegrated) tori embedded in chaotic seas. This enables a systematic strategy for transport studies.

The generic topological make-up of the basic ACEO flow is upheld for more complex ACEO systems, including combination with other forcing, in that flow topologies remain composed of (multiple) families of tori embedded in (interconnected) chaotic seas. Primary manifestation of more elaborate electrode layout/actuation and introduction of other

forcing is a more complex arrangement of the same elementary building blocks that admits systematic manipulation (within bounds of Hamiltonian dynamics) by way of actuation scenario of the electrodes and relative strength of possible additional forcing. This – in principle – facilitates creation of tailor-made Lagrangian flow structures for various transport purposes, ranging from pumping via targeted (spatio-temporal) entrapment to mixing. This may greatly enhance the functionality and versatility of labs-on-a-chip.

References

Aref H 2002 The development of chaotic advection *Phys. Fluids* **14** 1315

Bajer K 1994 Hamiltonian formulation of the equations of streamlines in three-dimensional steady flows *Chaos, Solitons Fractals* **4** 895

Bajer K and Moffatt H K 1990 On a class of steady confined Stokes flows with chaotic streamlines *J. Fluid Mech.***212** 337

Bazant M Z and Ben Y 2006 Theoretical prediction of fast 3D AC electro-osmotic pumps *Lab Chip* **6** 1455

Canuto, C, Hussaini, M Y, Quarteroni, A and Zang, T A 1988 Spectral Methods in Fluid Dynamics. Springer, Berlin

Cartwright J H E, Feingold M and Piro O 1996 Chaotic advection in three-dimensional unsteady incompressible laminar flow *J. Fluid Mech.* **316** 259

Chen J-K, Weng C-N and Yang R-J 2009 Assesment of three AC electroosmotic flow protocols for mixing in microfluidic channel *Lab on a Chip* **9** 1267

Hunt J C R 1965 Magnetohydrodynamic flow in rectangular ducts *J. Fluid Mech.* **21** 577

Kim B J, Yoon S Y, Lee K H and Sung H J 2010 Development of a microfluidic device for simultaneous mixing and pumping *Exp. Fluids* **46** 85

Kuo C-T and Liu C-H 2008 A novel microfluidic driver via AC electrokinetics *Lab on a Chip* **8** 725

Mills P L, Quiram D J and Ryley J F 2008 Microreactor technology and process miniaturization for catalytic reactions. A perspective on recent developments and emerging technologies *Chem. Eng. Sci.* **62** 6992

Neishtadt A I and Vasiliev A A 1999 Change of the adiabatic invariant at a separatrix in a volume-preserving 3D system *Nonlinearity* **12** 303

Nguyen N-T and Wu Z 2005 Micro-mixers—a review *J. Micromech. Microeng.* **15** R1

Ottino J M and Wiggins S 2004 Introduction: mixing in microfluidics *Phil. Trans. R. Soc.* A **362** 923

Ramos A, Morgan H, Green N G, González A and Castellanos A 2005 Pumping of liquids with travelling–wave electroosmosis *J. Appl. Phys.* **97** 084906

Speetjens M F M, Clercx H J H and van Heijst G J F 2004 A numerical and experimental study on advection in three-dimensional Stokes flows *J. Fluid Mech.* **514** 77

Speetjens M, Metcalfe G and Rudman M 2006a Topological mixing study of non-Newtonian duct flows *Phys. Fluids* **18** 103103

Speetjens M F M, Clercx H J H and van Heijst G J F 2006b Merger of coherent structures in time-periodic viscous flows *Chaos* **16** 043104

Speetjens, M. F. M., de Wispelaere, H. N. L., van Steenhoven, A.A. 2011 Multi-functional Lagrangian flow structures in three-dimensional AC electro-osmostic micro-flows Fluid. Dyn. Res. 43, 035503.

Squires T M 2009 Induced charge electrokinetics: fundamental challenges and opportunities *Lab on a Chip* **9** 2477

Stone H A, Stroock A D and Ajdari A 2004 Engineering flows in small devices: microfluidics toward a lab-on-a-chip *Annu. Rev. Fluid Mech.* **36** 381

Urbanski J P, Levitan J A, Burch D N, Thorsen T and Bazant M Z 2007 The effect of step height on the performance of three-dimensional AC electro-osmotic microfluidic pumps *J. Colloid Interface Sci.* **309** 332

Weigl B, Domingo G, Labarre P and Gerlach J 2008 Towards non- and minimally instrumented, micro-fluidics-based diagnostic devices *Lab on a Chip* **8** 1999

Wiggins S and Ottino J M 2004 Foundations of chaotic mixing *Phil. Trans. R. Soc.* A **362** 937